2D ATMOSPHERIC ARTIFACT COMPENSATION WITH MULTIPLE REGRESSION MODEL IN GROUND-BASED SAR OVER MOUNTAINOUS AREAS

X. Fabregas[(1)], R. Iglesias [(1)(2)], A. Aguasca[(1)], J. Gili[(2)]

[(1)] Universitat Politècnica de Catalunya, Departament de Teoria del Senyal i Comunicacions. D3 - Campus Nord, UPC, Barcelona, Spain. E-mail: fabregas@tsc.upc.es, ruben.iglesias@tsc.upc.edu, aguasca@tsc.upc.edu,

[(2)] Universitat Politècnica de Catalunya, Departament d'Enginyeria del Terreny, Cartogràfica i Geofísica. D2 - Campus Nord, UPC, Barcelona, Spain. E-mail: j.gili@upc.edu

ABSTRACT

This paper proposes a new technique for Atmospheric Phase Screen (APS) compensation based on a 2D Multiple Regression Model (height-dependent) in Ground-Based (GB) zero-baseline synthetic aperture radar (SAR) acquisitions over mountainous areas with steep topography. For this purpose, polarimetric measurements acquired using the GB-SAR sensor developed at the Universitat Politècnica de Catalunya (RISKSAR) are employed. This technique has been applied in the mountainous environment of Canillo in Andorra where there is an active landslide that nowadays is being reactivated coinciding with strong rains. Data sets are being acquired at X-band during one-year measuring campaign (October 2010 – October 2011). The effects of the atmosphere variations between successive campaign acquisitions and the way to compensate it are treated here in detail. The need to compensate for the resulting phase-difference errors when retrieving interferometric information is put forward. A new compensation technique is then proposed and evaluated using the control points placed inside the observed scene atmospheric artifact compensation in presence of steep topography.

1. INTRODUCTION

Differential SAR Interferometry (DInSAR) algorithms have been developed during the last 10 years showing their validity for monitoring deformation episodes, with millimetric precisions as well for providing a useful technique for their geophysical interpretation. In this context, and in those cases when wide area of observation is required, the use of satellite systems has been proven to be successful. An alternative solution, in some cases complementary, comes from the use of GB-SAR sensors [1], [2]. GB-SAR DInSAR is a remote sensing technique in which the high stability of the sensor platform, the lack of revisiting-time constrains and its high resolution possibilities are translated as a promising alternative to a satellite based solution when small scenarios are considered. The most relevant decorrelation source for targets that exhibit stable phase behavior in these types of data is the atmospheric phase screen [3]. In order to apply any differential interferometric technique for the deformation map retrieval, the atmospheric effects must be compensated. In Section 2, a general description of the system and the data-processing chain is given. In Section 3, we describe the test site selected for the field campaign. Section 4 shows how in areas with steep topographic variations, fluctuations of atmospheric parameters as temperature, pressure and humidity can be observed on the spatial domain for each acquisition mainly due to changes in height and how the assumption of atmosphere spatial homogeneity (constant refractivity index for the whole scene) fails. The results of numerical to these physical quantities are also included. In view of all these evidences, a 2D height-dependent new model to estimate the APS is presented.

2. SYSTEM DESCRIPTION

Unlike the most of the other GB-SAR systems available in the remote sensing scientific community, which are based on a Vector Network Analyzer (VNA) for the stepped-frequency sweeping of the transmitted signal bandwidth [4], the UPC CW-FM radar is based on a Digital Direct Synthetizer (DDS) chipset that generates it at once. This kind of solution allows performing polarimetric measurements without increasing the temporal decorrelation effects during a single scan and this extra information, for instance, will provide higher densities to phase atmosphere estimation and removal. The processing algorithm consists of two mains steps: Raw Data are first range-compressed by a fast Fourier transform (since the system works in the time domain [5]) and then focused in the cross-range direction by a backprojection technique [6]. Despite its time-consuming performance, this algorithm can easily take into account the fact that the cross-range resolution is not a constant parameter in the GB-SAR images [7].

3. TEST SITE DESCRIPTION

The Remote Sensing Laboratory (RSLab) in collaboration with The Department of Geotechnical Engineering and Geosciences of the Universitat Politècnica de Catalunya (UPC) is carrying out a one-year measuring campaign (October 2010 – October 2011) in the landslide of 'El Forn de Canillo', Andorra

Proc. 'Fringe 2011 Workshop', Frascati, Italy,
19–23 September 2011 (ESA SP-697, January 2012)

(see Fig. 1), using the polarimetric UPC GB-SAR sensor (RISKSAR) [4]. This work is being carried out in the frame of the fourth area of Safeland project funded by The Seventh Framework Program for research and technological development (FP7) of the European Commission. 'El Forn de Canillo' is an ancient landslide with a complex movement that took place in more than one episode.

The landslide of 'El Forn de Canillo' constitutes one of the biggest landslides of the Pirenaic area. It is an ancient landslide with a complex movement that took place in more than one episode. Nowadays it is quite stable, with some residual movement (of the order of millimeters per year). Some profiles show that it might produce local slides for situations as big excavations, undermining by erosion, important ascents of the groundwater level in extraordinary periods of rainfall. In the North-East extreme of the landslide of 'El Forn Canillo' exists a sector that nowadays is active and it is reactivated coinciding with strong rains and big increases of the piezometric conditions episodes of the zone. In paricular, it is the secondary landslide of Cal Borró - Cal Ponet what during the period of snow merging and major rainfalls frequency (during May and June 2009 deformations have been observed of between 2-3 cm / month) [8].

Figure 1. Panoramic view of 'El Forn de Canillo'

4. ATMOSPHERIC ARTIFACT ANALYSIS OVER MOUNTANIOS AREAS

One of the benefits of using the GB-SAR sensor is the possibility of acquiring zero-baseline repeated images for differential measurements. Many effects of decorrelation that normally affect the differential coherence such as corregistration errors, baseline constructions uncertainties, and digital elevation model removal residual errors, are negligible here. The expression of the differential interferometric coherence is defined by:

$$\gamma = \left|\gamma_t \gamma_{th}\right| e^{j\phi} \tag{1}$$

where γ_t represents the temporal decorrelation due to the fact that SAR images have been acquired at different time and γ_{th} depends on the signal to noise ratio (SNR). The thermal noise contribution to γ degradation is low because of the high-power transmitted signal. Therefore, temporal decorrelation is the major decorrelation source in measurements and consequently γ can be described in terms of temporal decorrelation. The phase can be directly translated into an equivalent along-range displacement:

$$\Delta\phi = \frac{4\pi}{\lambda}\Delta r \rightarrow \Delta r = \frac{\lambda}{4\pi}\Delta\phi \tag{2}$$

where Δr can be interpreted as a physical movement of the target under the hypothesis that the propagation properties in the medium are the same along the two acquisitions. In all most cases, the hypothesis fails and it is the consequence that generates the atmospheric artifacts.

Therefore, APS represents the major responsible for the severe phase fluctuations in the received signal and represents the major GB-SAR decorrelation source in measurements. In order to apply any DInSAR technique for deformation map retrieval, the estimation and removal of the APS from the data is the key point of the data processing.

A simple model explaining their physical existence is based on the modulation of the velocity of an electromagnetic wave through a homogeneous medium by the index of refraction n. In the GB-SAR case, the medium is the troposphere, and n strictly depends on temperature T (in kelvin), pressure p (in millibars), and humidity h (percent per hundred) at each point, as pointed out by the following semiempirical expression [9]:

$$n = n(T, p, h) = 1 + (N_{dry} + N_{wet}) \cdot 10^{-6} \tag{3}$$

where the Nwet and Ndry components are defined by:

$$\begin{aligned} \mathrm{N_{dry}} &= \frac{77.6 \cdot p}{T} \\ \mathrm{N_{wet}} &= \frac{3.73 \cdot 10^5 \cdot w_p}{T^2} \end{aligned} \tag{4}$$

w_p is the water vapor pressure in mb and is usually derived from the relative humidity. Defining the maximum possible (saturated) vapor pressure at the temperature T as w_{ps}, w_p it given by

$$w_p = w_{PS} H = 6.11 e^{\left(19.7 \frac{T-273}{T-2 \cdot 273}\right)} H \tag{5}$$

N_{dry} and N_{wet} strictly depend on the temperature T but separate the effect of the relative humidity. For example for a very low temperature N_{wet} becomes very small even for saturated air and the index of refraction is

almost independent of H. As the temperature rises, there is a slow decrease of N_{dry} but a rapid increase of N_{wet}. The dry component is the larger of both but the wet refractivity presents major problems because it causes major variations between close consecutive acquisitions. The relationship between the index of refraction and the refractivity index is

$$n=\left(N\cdot 10^{-6}\right)+1 \tag{6}$$

and it is a spatiotemporal function of each image acquisition.

$$n=n(T(\vec{r},t),P(\vec{r},t),H(\vec{r},t))=n(\vec{r},t) \tag{7}$$

The absolute phase of n^{th} target using a monochromatic wave at frequency f_c in the instant t is composed by its own backscatter phase φ_0, by the propagation delay term proportional to the distance r_n between the target and the sensor and a phase term due to the APS [10].

$$\varphi_n(t)=\varphi_0+\frac{4\pi f_c}{c}\left(r_n+\varphi_{ATM,n}(t)\right) \tag{8}$$

The atmospheric phase due to the non-idealities of the troposphere can be obtained through the result from the integration of the refractivity function along the path L which links the radar to the target and can be expressed as

$$\varphi_{ATM,n}(t)=10^{-6}\cdot\frac{4\pi f_c}{c}\int_L N(\vec{r},t)dl \tag{9}$$

This general formulation of absolute phase shows that the APS is a space-time dependent function.

Under the assumption of atmosphere spatial homogeneity (constant refractivity index for the whole scene), which has been demonstrate that works perfectly in smooth topography environments, the refractivity index N does not change with range distance and remain constant along the time interval that the wave needs to go and back from the sensor to the target.

Therefore, under spatially homogeneity assumption the Eq. 9 can be rewritten as

$$\varphi_{ATM,n}(t)=10^{-6}\cdot\frac{4\pi f_c r_n N(t)}{c} \tag{10}$$

Thus, the differential phase we are interested in can be expressed under different atmospheric conditions at times t_1 and t_2 as follows

$$\Delta\varphi_n(t_1,t_2)=\varphi_n(t_2)-\varphi_n(t_1)=\varphi_{ATM,n}(t_2)-\varphi_{ATM,n}(t_1)$$
$$\frac{4\pi f_c r_n}{c}\cdot\left(N(t_2)-N(t_1)\right)=\frac{4\pi f_c r_n}{c}\cdot\Delta N \tag{11}$$

The differential phase $\Delta\varphi_n$ increases linearly with range distance and the atmosphere artifact estimation consists of a linear range phase. The projection onto a range-line of the phase of all the pixels whose coherence values are higher than a reference threshold shows a linear behavior due to the atmosphere spatial homogeneity. In these conditions, the atmospheric phase contribution may be compensated with a regression-line estimator [11].

In scenes with steep topographic variations, fluctuations of atmospheric parameters as temperature, pressure and humidity can be observed on the spatial domain for each acquisition mainly due to changes in height. This aspect produces refractive index changes with r, which means it varies in space (height) and in time for each acquisition. By denoting with h the height above the ground, the distribution of the refractive index N through the whole troposphere is hence modeled as a multi-layer medium and its decrease is described as [9]

$$N(h)=N_0\cdot e^{-\alpha h} \tag{12}$$

where N_0 is the value of the refractive index at the sea level and α is the height scale inverse. For small scenarios the refractivity index can be approximated by the first two terms of Taylor series due to its linear behavior in short distances:

$$N(h)=N_0-N_0\cdot\alpha\cdot h=N_0+N_1\cdot h \tag{13}$$

In the Fig. 2 it is shown the linear behavior of the refractivity index obtained from meteorological measurements profiles of pressure, temperature and relative humidity collected by a weather station along different spatial points with different heights of the hillside.

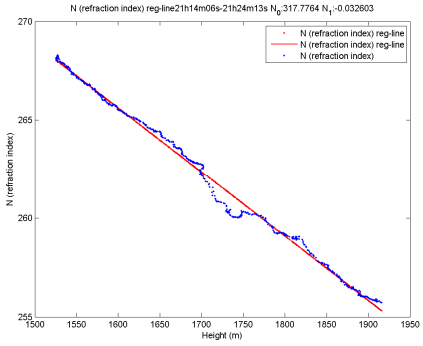

Figure 2. Linear behaviour approximation of N in steep topography scenarios.

Defining h_n' as the total height above sea level of the n^{th} target, h_r as the GB-SAR sensor height and h_n as the relative target height between the n^{th} target and the GB-SAR sensor

$$h_n^{'} = h_r + h_n \tag{14}$$

The Eq. 9 can be rewritten as follows

$$\varphi_{ATM,n}(t) = 10^{-6} \cdot \frac{4\pi f_c}{c} \int_L N(\vec{r},t)dl = \frac{4\pi f_c}{c} \cdot 10^{-6} \cdot \left(\left(N_0(t) + N_1(t) \cdot h_R \right) r_n + \frac{1}{2} N_1(t) \cdot r_n^2 \cdot \sin\theta_n \right) \tag{15}$$

where θ_n is the angle of observation of the n^{th} target. The absolute phase due to atmospheric disturbances presents now a quadratic behavior with range.
In the steep topography situation the troposphere stops behaving as a homogeneous medium and it better described by a multi-layer model. In general, propagation of electromagnetic plane waves through a multilayer medium generates phenomena known as ray-banding. However, the apparent displacements are low, especially in the near-range, and this term can be neglected doing the following approximation

$$h_n = r_n \cdot \sin\theta_n \tag{16}$$

Then, the Eq. 15 can be rewritten by

$$\varphi_{ATM,n}(t) = \frac{4\pi f_c}{c} \cdot 10^{-6} \cdot \left(\left(N_0(t) + N_1(t) \cdot h_R \right) r_n + \frac{1}{2} \cdot N_1(t) \cdot r_n \cdot h_n \right) \tag{17}$$

The equation can be interpreted as the sum of two contribution terms. The first term increases linearly with range as in the case of spatial homogeneity and a second term appears with height-dependency.
Finally, under different atmospheric conditions at times t_1 and t_2 the differential phase $\Delta\varphi$ can be expressed as

$$\Delta\varphi_n(t_1,t_2) = \varphi_n(t_2) - \varphi_n(t_1) = \varphi_{ATM,n}(t_2) - \varphi_{ATM,n}(t_1) \beta_0 + \beta_1 \cdot r_n + \beta_2 \cdot h_n \cdot r_n \tag{18}$$

where β_0 is an offset that can appear between different campaigns measurements due to the change of initial conditions and

$$\beta_1 = \frac{4\pi f_c}{c} \cdot 10^{-6} \cdot \left(\Delta N_0(t_1,t_2) + \Delta N_1(t_1,t_2) \cdot h_R \right)$$
$$\beta_2 = \frac{4\pi f_c}{c} \cdot 10^{-6} \cdot \left(\frac{1}{2} \Delta N_1(t_1,t_2) \right) \tag{19}$$

The consequence is that under steep topography conditions the atmosphere spatial homogeneity cannot be considered and any linear model approximation solution fails due to the quadratic behavior of the differential phase $\Delta\varphi$ (see Fig. 3).

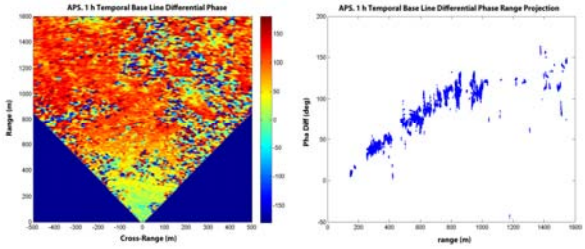

Figure 3. APS measured in 1h Temporal Base Line (right). Range projection of APS (left). We can see second-order term in the differential interferometric phase which depends on the range distance and height.

5. MULTIPLE REGRESSION MODEL COMPENSATION

A new model to estimate the APS has to be considered under this type of scenarios with steep topography. Considering the new expression of the differential phase $\Delta\varphi$, the observation variables can be defined as follows

$$x_{i1} = r_i \; ; x_{i2} = h_i \cdot r_i \tag{20}$$

The differential phase $\Delta\varphi$ can be expressed for a single spatial point i as a general lineal model [12]

$$\Delta\varphi_{ATM\,i} = \beta_0 + \beta_1 \cdot r_i + \beta_2 \cdot h_i \cdot r_i = \beta_0 + \beta_1 \cdot x_{i1} + \beta_2 \cdot x_{i2} \tag{21}$$

Given a random sample of observations of differential phase $\Delta\varphi_1$, $\Delta\varphi_2$, …, $\Delta\varphi_1$, at the observation points, x_{11}, x_{12}, ..., x_{1k}, x_{21}, x_{22}, ..., x_{2k}, x_{n1}, x_{n2}, ..., x_{nk}, respectively, based on the general linear model, we have the following n equations

$$\begin{cases} \Delta\varphi_1 = \beta_0 + \beta_1 x_{11} + \beta_2 x_{12} + \varepsilon_1 \\ \Delta\varphi_2 = \beta_0 + \beta_1 x_{21} + \beta_2 x_{22} + \varepsilon_2 \\ \ldots \\ \Delta\varphi_n = \beta_0 + \beta_1 x_{n1} + \beta_2 x_{n2} + \varepsilon_n \end{cases} \tag{22}$$

where ε_1, ε_2, .. ε_n are the random errors of observations. The general lineal model can be expressed compactly in matrix form as follows

$$\mathbf{\Delta\varphi = X\beta + \varepsilon} \tag{23}$$

where

$$\boldsymbol{\Delta\varphi} = \begin{bmatrix} \Delta\varphi_1 \\ \Delta\varphi_2 \\ \vdots \\ \Delta\varphi_n \end{bmatrix},\ \mathbf{X} = \begin{bmatrix} 1\, x_{11}\ x_{12} \\ 1\, x_{21}\ x_{22} \\ \vdots\ \vdots\ \vdots \\ 1\, x_{n1}\ x_{n2} \end{bmatrix},\ \boldsymbol{\beta} = \begin{bmatrix} \beta_0 \\ \beta_1 \\ \beta_2 \end{bmatrix},\ \boldsymbol{\varepsilon} = \begin{bmatrix} \varepsilon_1 \\ \varepsilon_2 \\ \vdots \\ \varepsilon_n \end{bmatrix} \quad (24)$$

where **X** is a matrix of n x 3 with the observation variables, **β** is a vector with the unknown parameters of 3 x 1, and **Δφ** and **ε** are vectors of n x 1, containing the observations of differential phase and the random errors. The unknown parameters vector **β** can be obtained from least squares by the following equation [12]

$$\boldsymbol{\beta} = \left(\mathbf{X}'\mathbf{X}\right)^{-1}\mathbf{X}'\boldsymbol{\Delta\varphi} \quad (25)$$

where ' indicates the transposed conjugate of the data.
The estimated equation of the Multiple Regression Model is

$$\widehat{\boldsymbol{\Delta\varphi}}_{MRM} = \mathbf{X}\boldsymbol{\beta} \quad (26)$$

To avoid noisy measures in the Multiple Regression Model estimation a selection of high coherent pixels of the motionless area must be done to filter out the unreliable points corrupted by the temporal decorrelation.
In another hand, to perform this compensation technique it is need information of the height. Using an external DEM and solving the Multiple Regression Model in the high coherence points of the interferogram the APS can be estimated and removed by the following way

$$\Delta\varphi_{COMP} = \Delta\varphi \cdot e^{j\widehat{\Delta\phi}_{MRM}} \quad (27)$$

In the particular case of smooth topography this new model trends to the 1D phase-ramp solution so it is a generalization of the linear model approximation.
In the Fig. 4 it is shown the APS compensation process for a one hour time-baseline interferogram of a campaign corresponding to November 2010. It can be noticed the height-dependency of the estimated Multiple Regression Model (left-up corner) due to the non-spatially homogeneity of the refractivity index. In the right-up corner it is shown the polarimetric zero-baseline interferometric phase after compensating the atmospheric artifacts. We can observe the zero mean value of the resulting differential phase revealing the proper functioning of the new estimation technique due to the absence of motion in one hour measurement interval. In the left-down corner it is shown the distribution of the differential phase pixels and the Multiple Regression Model in high-coherent pixels (threshold =0.97) projected on a single range-cut. It can be noticed the non linear behavior of atmospheric disturbances and the perfect adjustment of the model. Finally, it is shown the range-cut projection of the resulting compensated differential phase (right-down corner) revealing again the zero-mean resulting compensated differential phase due to the absence of movement within a single campaign.
In the Fig. 5 it is shown the geocoded differential phase in high-coherent pixels (threshold =0.97) projected in a Google earth image (left) and the compensated differential interferogram (right) with the Multiple Regression Model. Again after the compensation the differential phase is expected to be zero mean because of the absence of movement.

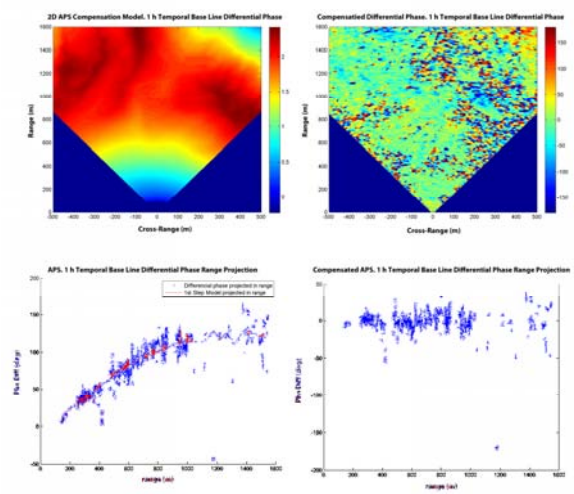

Figure 4. 2D Multiple Regression Model (left-up corner). Zero mean compensated differential phase (right-up corner). Single range-cut projection of APS and Multiple Regression Model in high-coherent pixels, threshold =0.97 (left-down corner). Single range-cut projection zero mean compensated differential phase in high-coherent pixels, threshold =0.97 (right-down corner).

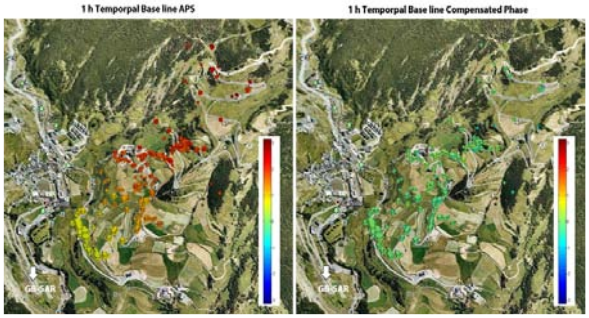

Figure 5. APS in points with coherence greater than 0.97 threshold gecoded in a google earth image (left). Compensated differential interferogram (right). After compensation the differential phase is expected to be zero mean because of the absence of movement.

6. LONG TIME ATMOSPHERIC PHASE SCREEN COMPENSATION

The landslide of Canillo is nowadays quite stable and it is expected to have some residual movement of the order of few millimeters per year, therefore continuous monitoring clearly results unfruitful. Many separated interferograms with high temporal baseline will be performed from images of the reference campaign and images of the latter campaign.

The estimation of the atmospheric phase artifacts in long time span zero-baseline GB-SAR between different campaign acquisitions has to be compensated with the minimum loose of coherence. It is a key point because the higher the density of coherent scatters the better the estimation of the APS. Following this main reasoning, it is possible to create a set of short-time compensation functions between consecutive campaigns defined as [13]

$$F_{w,w+1} = e^{j\widehat{\Delta\varphi}_{w,w+1}} = \\ = e^{j(\beta_0+\beta_1\cdot r_n+\beta_2\cdot h_n\cdot r_n)} \quad (28)$$

Hence, the compensating function of the l,m interferogram is obtained by simply multiplying the m, l-1 basis functions from campaign l to campaign m as follows [13]

$$F_{l,m} = \prod_{w=l}^{m-1} F_{w,w+1} \quad (29)$$

The 0B compensated interferometric phase $\Delta\varphi_{l,m}$ obtained from the time-averaged acquisitions of campaign l and m is hence given by [13]

$$\Delta\varphi_{l,m}(i,j) = \frac{\left|\sum_{i=0}^{L_1-1}\sum_{j=0}^{L_2-1} S_l(i,j)\cdot S_m^*(i,j)\cdot F_{l,m}^*\right|}{\sqrt{\left(\sum_{i=0}^{L_1-1}\sum_{j=0}^{L_2-1}\left|S_l(i,j)\right|^2\right)\left(\sum_{i=0}^{L_1-1}\sum_{j=0}^{L_2-1}\left|P_m(i,j)\right|\right.}} \quad (30)$$

where $N = L_1 \times L_2$ is the number of looks of the boxcar used to estimate the coherence and S_l and S_m are the complex values from two pixels of the first and second acquisition image used to perform the interferogram, * indicates the complex conjugate.

Therefore, the APS basis functions F_i are obtained from consecutive daily-averaged GB-SAR acquisitions where the deformation contribution can be assumed negligible and are linearly combined to cope with the artifact compensation in any time-span GB-SAR differential interferogram.

The blocks-diagram of Fig. 6. resumes the whole processing chain.

After compensating the atmospheric artifacts $\binom{N}{2}$ interferograms will be generated from the N available time-averaged images.

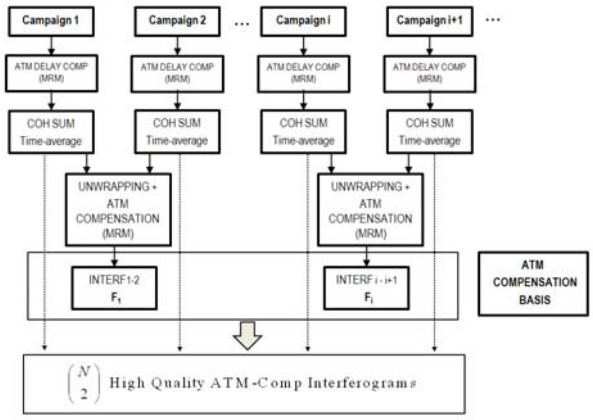

Figure 6. Pre-processing chain for the estimation of the atmospheric phase artefacts in long time span zero-baseline GB-SAR acquisitions. The basic functions Fi are obtained from consecutive daily-averaged GB-SAR acquisitions where the deformation contribution can be assumed negligible and are linearly combined to cope with the artefact compensation in any time-span GB-SAR differential interferogram.

7. First DInSAR RESULTS

First results show that nowadays the landslide is quite stable, with some residual movement of the order of few millimeters per year.

As preliminary results it is shown an interferogram formed by daily-averaged GB-SAR acquisitions corresponding to October 2010 - May 2011 after doing Multiple Regression Model compensation of APS. It have been used high-coherent pixels (threshold =0.97) and a Multilook of 15x15. Some profiles show that it might produce local slides for situations as big excavations, undermining by erosion, important ascents of the groundwater level in extraordinary periods of rainfall. In the North-East extreme of the landslide of 'El Forn Canillo' exists a sector that nowadays is active and it is reactivated coinciding with strong rains with a maximum motion rate movement of the order of 1.5 cm per year (see Fig. 7).

The Department of Geotechnical Engineering and Geosciences of the UPC will perform in the future a geological analysis and interpretation of the results making a cross comparison of the radar deformation maps with in-field measurements (inclinometers, extensometers).

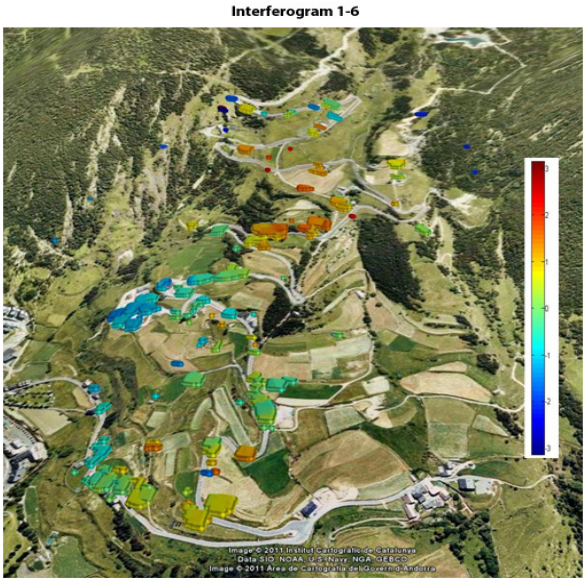

Figure 7. Interferogram of campaigns corresponding to October 2010 - May 2011. In the figure are represented these points with a coherence greater than 0.85 using a Multilook 15x15. The stable zone is represented with blue colour and the maximum deformation is indicated with the red colour representing a deformation of 1.5 cm.

8. CONCLUSIONS

In this paper, the effects in a monotonous area of atmosphere changes in the zero baseline GB-SAR measurements at X-band have been analyzed. Under steep topography areas conditions atmosphere spatial homogeneity cannot be considered and any linear model approximation solution fails. A coherence-based 2D Multiple Regression Model high-dependent procedure for the removal of the deriving phase artifacts has been proposed and tested in simulated and real data. The acquisition time has turned out to be the key factor in the GB-SAR acquisitions: it must be reduced as much as possible to guarantee the medium homogeneity hypothesis and to model the distortion phenomenon. Otherwise, the atmosphere instability can prevent this condition to be fulfilled and lead to unpredictable and, sometimes, not removable distortion effects.

ACKNOWLEDGMENTS

This research work received partial support from the Safeland project funded by the Commission of the European Communities (grant agreement 226479), from the Big Risk project (contract number BIA2008-06614) and TEC Project (TEC2008-06764-C02-01) funded by the Spanish MICINN.

REFERENCES

1. Leva, D., Nico, G., Tarchi, D., Fortuny-Guash, J. and J. Siber, A. (2003). Temporal analysis of a landslide by means of a ground-based SAR interferometer. *IEEE Trans. Geosci. Remote Sens.* **41** (4), 745–752.

2. Tarchi, D., Rudolf, H., Pieraccini, M. and Atzeni, C. (2000). Remote monitoring of buildings using a ground-based SAR: Application to cultural heritage survey. *Int. J. Remote Sens.* **21**(18) 3545–3551.

3. Pipia, L., Aguasca, A., Fabregas, X., Mallorqui, J.J. and Lopez-Martinez., C. (2005). Temporal Decorrelation in Polarimetric Differential Interferometry using a Ground-Based SAR Sensor. *Proc. IGARSS'05*, Seul,Korea, pp25-29.

4. Aguasca, A., Broquetes, A., Mallorqui, J.J. and Fabregas, X. (2004). A Solid State L to X-band Flexible Ground-based SAR System for Continuous Monitoring Applications. *Proc. IGARSS'04*, Anchorage, Alaska, pp757-760.

5. Pipia, L., Aguasca, A., Fabregas, X. and Mallorqui, J.J. (2005). A polarimetric ground-based SAR system: First results at X-band. in Proc. *Proc. URSI Commission F Symp. Microw. Remote Sens. Earth, Oceans, Ice, Atmosphere*, Ispra, Italy, pp20–21.

6. Ulander, H., Hellsten, H. and Tenström, G.S. (2003). Synthetic-aperture radar processing using fast factorized backprojection. *IEEE Trans. Aerosp. Electron. Syst.*. **39**(3) pp760–776.

7. Soumekh, M. (1999) *Synthetic Aperture Radar Signal Processing*. NewYork: Wiley.

8. Torrebadella, J., Villaró, I., Altimir, J., Amigó, J., Vilaplana, J.M., Corominas, J. and Planas, X. (2009). El Deslizamiento del Forn de Canillo en Andorra. Un Ejemplo de Gestión del Riesgo Geológico en Zonas Habitadas en Grandes Deslizamientos. *VII Simposio Nacional sobre Taludes y Laderas Inestables*.

9. Hall, M.P. (1979). *Effects of the Troposphere on Radio Communication*. The Institution of Electrical Engineers, London.

10. Iannini, L. and Monti Guarnieri, A. (2011). Atmospheric Phase Screen in Ground-Based Radar: Statistics and Compensation. *Geoscience and Remote Sensing* Letters, IEEE 8(3), 537-541.

11. Pipia, L., Fabregas, X., Aguasca, A. and Lopez-Martinez., C. (2008). Atmospheric Artifact Compensation in Ground-Based DInSAR Applications. *Geoscience and Remote Sensing Letters, IEEE* **5**(1), 88-92.

12. Canovos, C. (1999). *Applied Probability and Statistical Methods.* McGraw-Hill.

13. Pipia, L. (2009). *Polarimetric Diferential SAR Interferometry with Ground-Based sensors*. PhD Dissertation,Universitat Politècnica de Catalunya, Barcelona.